Vol 16 No 4, April 2007
1009-1963/2007/16(04)/1089-08

Chinese Physics

© 2007 Chin. Phys. Soc.
and IOP Publishing Ltd

Numerical studies of atmospheric pressure glow discharge controlled by a dielectric barrier between two coaxial electrodes*

Zhang Hong-Yan(张红艳）, Wang De-Zhen(王德真)†, and Wang Xiao-Gang(王晓钢）

State Key Laboratory of Materials Modification by Laser, Electron, and Ion Beams,

School of Physics and Optoelectronic Technology, Dalian University of Technology, Dalian 116024, *China*

(Received 30 May 2006; revised manuscript received 20 October 2006)

The glow discharge in pure helium at atmospheric pressure, controlled by a dielectric barrier between coaxial electrodes, is investigated based on a one-dimensional self-consistent fluid model. By solving the continuity equations for electrons, ions, and excited atoms, with the current conservation equation and the electric field profile, the time evolution of the discharge current, gas voltage and the surface density of charged particles on the dielectric barrier are calculated. The simulation results show that the peak values of the discharge current, gas voltage and electric field in the first half period are asymmetric to the second half. When the current reaches its positive or negative maximum, the electric field profile, and the electron and ion densities represent similar properties to the typical glow discharge at low pressures. Obviously there exist a cathode fall, a negative glow region, and a positive column. Effects of the barrier position in between the two coaxial electrodes and the discharge gap width on discharge current characteristics are also analysed. The result indicates that, in the case when the dielectric covering the outer electrode only, the gas is punctured earlier during the former half period and later during the latter half period than other cases, also the current peak value is higher, and the difference of pulse width between the two half periods is more obvious. On reducing the gap width, the multiple current pulse discharge happens.

Keywords: dielectric barrier discharges, atmosphere pressure glow discharge, plasma, numerical simulation

PACC: 5256, 7750, 5280D, 5280H

1. Introduction

Traditional ways to produce plasmas at the atmospheric pressure include arc, corona, and dielectric barrier discharges, etc. In an arc discharge, thermal plasmas are yielded, which are mainly applied in metallurgy, spray and cutting. In corona and dielectric barrier discharges, the gas temperature is very low and nonthermal equilibrium plasmas are formed. The plasmas produced by corona discharge are usually confined in a small region near the electrode and limited to the application in materials processing. The dielectric barrier discharge at atmospheric pressure can exhibit a homogeneous diffuse mode under special conditions, which is called the atmospheric pressure glow discharge (APGD) due to its great similarity to the glow discharge at low pressure. Since APGD produces homogeneous non-equilibrium plasmas, it leads to a broad prospect in applications including materials modification, thin-film deposition, etching, sterilization and disinfection of medical apparatus, fibre modification and so on.

In recent years, APGD has become one of the main research focuses in low-temperature plasma studies. Okazaki *et al*[1−3] have first reported a technique in generating the APGD by using dielectric barriers, with AC fields. Roth and his group[4−6] have independently started to study the dielectric barrier discharge at atmospheric pressure, as well as to apply it to disinfection in medical apparatus, fibre modification, thin-film deposition and so on. Massines and co-workers[7,8] have developed the experimental and numerical study on APGD and their results show that APGD has similar characteristics to those of the glow discharge at low pressures. Kong and Deng [9] put forward a new way of using pulse-voltage to generate APGD. Close attention has been paid by researchers to generate APGD controlled by a dielectric barrier between parallel-plate electrodes.[10−12] The experimental and numerical simulation stud-

*Project supported by the National Natural Science Foundation of China (Grant Nos 50537020 and 50528707).

†E-mail: wangdez@dlut.edu.cn

ies about this kind of discharge configurations are widely developed.[13−16] However, studies in the area of APGD or plasma jets generated between coaxial electrodes are relatively rare.[17,18]

In this paper, we present a numerical simulation of APGD by the dielectric barrier situated between two coaxial electrodes. Solving the continuity equations for electrons, ions, and excited particles, also the current conservation equation, we have calculated the distributions of the electric field profile and the electron, ion and excited atom densities in the discharge area, as well as the temporal evolution of discharge current, gas voltage and surface charge densities accumulated on the insulated dielectric barrier.

2. Simulation model

The discharge we studied is generated between two coaxial electrodes. An outer grounded cylindrical electrode surrounds a quartz glass tube from outside, and a sinusoidal voltage is applied to the inner wire electrode at the axis of the cylinder ($r = 0$). The outer radius of the inner electrode isR_0, and the inner radii of the dielectric and the outer electrode are R_1 and R_2, respectively, as shown in Fig.1.

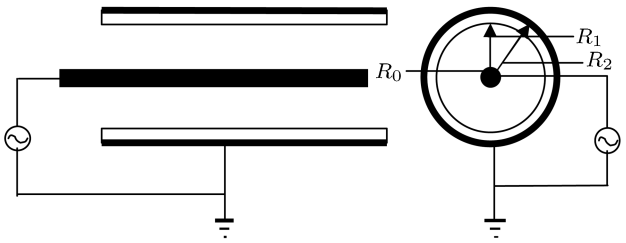


Fig.1. Dielectric barrier discharge configuration in an axial symmetry system.

Working gas used is pure helium. The numerical simulation is based on a one-dimensional and self-consistent fluid model. Under the condition of drift-diffusion approximation, continuity equations for the charged particles and excited atoms can be written as

$$\frac{\partial n_k}{\partial t} + \frac{1}{r}\frac{\partial (r j_k)}{\partial r} = S_k, \tag{1}$$

$$j_k = -D_k \frac{\partial n_k}{\partial r} + \mu_k n_k E, \tag{2}$$

where n_k, j_k, D_k, μ_k, S_k are density, flux, diffusion coefficient, mobility and source term for the kth species of particles, respectively, with t and r being time and the radial distance from the axis; E is the electric field, and the subscripts $k = e, i, a$ represent electrons, atomic and molecular ions, and excited atoms respectively. Especially, if $k = e$, the mobility μ is negative, and if $k = a$, the mobility μ equals zero.

Instead of Poisson's equation in our numerical simulation calculation, the electric field is given by the current conservation equation,

$$\varepsilon(r)\frac{\partial E(r,t)}{\partial t} + i_{\rm c}(r,t) = i_{\rm T}(r,t), \tag{3}$$

where the permittivity $\varepsilon(r)$ depends on the position. In the gas region, $\varepsilon(r) = \varepsilon_0$, and in the dielectric barrier, $\varepsilon(r) = \varepsilon_0\varepsilon_{\rm b}$, with $\varepsilon_{\rm b}$ being the relative permittivity. In Eq.(3) $i_{\rm T}(r,t)$ is the total discharge current density including the conductive current and the displacement current densities. The conductive current $i_{\rm c}$ is then given by

$$i_{\rm c}(r,t) = e(j_{\rm i}(r,t) - j_{\rm e}(r,t)), \tag{4}$$

where $j_{\rm i}(r,t)$ and $j_{\rm e}(r,t)$ are respectively the ion and electron fluxes given by Eq.(2). Taking the secondary electron emission into account, the conductive current at the surfaces of the inner electrode and the dielectric should be

$$i_{\rm c}(r,t) = e[j_{\rm i}(r,t) - (j_{\rm e}(r,t) + \gamma j_{\rm i}(r,t))], \tag{5}$$

with γ the secondary electron emission coefficient. In this paper, we mainly simulate the elementary discharge properties generated between the two coaxial electrodes and do not discuss the influences of the secondary electron emission coefficient on the discharge properties, therefore we assume $\gamma = 0.01$ at the cathode regardless of whether it is insulated. The electric field E should satisfy the following boundary condition:

$$\int_{R_0}^{R_2} E(r,t){\rm d}r = V_{\rm a}(t), \tag{6}$$

where $V_{\rm a}(t) = V_0 \sin(2\pi f t)$ is the sinusoidal external voltage applied to the inner electrode. Multiplying the both sides of Eq.(3) by $2\pi rL$, we can define the total discharge current as $I_{\rm T} = 2\pi rL \cdot i_{\rm T}$, which is independent of radius r, with L being the axial length of the discharge installment

$$2\pi rL \cdot \varepsilon(r)\frac{\partial E(r,t)}{\partial t} + 2\pi rL \cdot i_{\rm c}(r,t) = I_{\rm T}(t). \tag{7}$$

Integrating Eq.(7) over the discharge region, we can compute the total discharge current $I_{\rm T}(t)$,

$$I_{\rm T}(t) = \frac{2\pi L\varepsilon_0\varepsilon_{\rm b}}{[\varepsilon_{\rm b}\ln(R_1/R_0) + \ln(R_2/R_1)]} \times \Big[\frac{\partial V_{\rm a}(t)}{\partial t} + \frac{1}{\varepsilon_0}\int_{R_0}^{R_1} i_{\rm c}(r,t){\rm d}r\Big]. \tag{8}$$

From Eq.(8), we can obtain the total current density versus different radii by using the relation

$$i_{\mathrm{T}}(r,t) = \frac{I_{\mathrm{T}}(t)}{2\pi r L} = \frac{\varepsilon_0\varepsilon_{\mathrm{b}}}{r[\varepsilon_{\mathrm{b}}\ln(R_1/R_0)+\ln(R_2/R_1)]} \times \Big[\frac{\partial V_{\mathrm{a}}(t)}{\partial t} + \frac{1}{\varepsilon_0}\int_{R_0}^{R_1} i_{\mathrm{c}}(r,t)\mathrm{d}r\Big]. \quad (9)$$

The surface density of charged particles accumulated on the dielectric barrier is described as

$$\sigma_{\mathrm{b}}(t) = \int_0^t i_{\mathrm{c}}(R_1,t')\mathrm{d}t'. \quad (10)$$

The charged particles considered in the present model are the electron e, atomic ion He^+, and molecular ion He_2^+. Since at the atmospheric pressure, the states $He(2^1S)$ and $He(2^3S)$ of excited He atoms have very similar behaviours, so that they are often unified into one effective level expressed as He^*. The elementary ionization and excitation processes expressed in the source term are listed in Table 1. In the present calculation, electrons are assumed to be in equilibrium with the local electric field. In fact, electrons are not always in equilibrium with the local electric field, particularly in the sheath region.[24,25] However, the results obtained in the present study could provide a relatively clear picture of plasma dynamics. A quantitatively more accurate description can in principle be developed in a similar way to that reported recently in Ref.[26].

Table 1. The elementary reaction process in pure helium.

	Reaction	Rate constant	Reference
Direct ionization	e+ He → He^+ +2e	α	[19]
Excitation	e+ He → He^+ +e	$4.2\times10^{-9}T_{\mathrm{e}}^{0.31}\mathrm{e}^{-19.8/T_{\mathrm{e}}}$ cm^3/s	[20]
Ionization of metastable	e+ He^* → He^+ +2e	$1.28\times10^{-7}T_{\mathrm{e}}^{0.6}\mathrm{e}^{-4.78/T_{\mathrm{e}}}$ cm^3/s	[20]
Ion conversion	He^++ 2He → He_2^+ + He	2.0×10^{-31} cm^6/s	[20]
Penning ionization	He^* + He^* → e + He^+ + He	8.7×10^{-10} cm^3/s	[21]
	→ e + He_2^+	2.03×10^{-9} cm^3/s	
Dissociative recombination	He_2^+ + e → 2 He	4.0×10^{-9} cm^3/s	[22]
	He^+ + e → He	$8.1\times10^{-20}\frac{n_{\mathrm{e}}}{1+0.079p}(T_{\mathrm{e}}/T_{\mathrm{g}})^{-4.4}$ cm^3/s	[23]
De-excitation	He^* + e → He + e	2.9×10^{-9} cm^3/s	[21]

3. Results and discussions

In our model, the series of equations above are solved numerically, and the discretization of Eq.(1) is performed in accordance with semi-implicit Scharfetter–Gummel scheme.[27,28] The mobility and diffusion coefficient used are the same as those in Refs.[23], [29], and [30]. The photo-ionization contribution is not taken into account in this model. The secondary electron emission coefficient due to ion scattering at the cathode is assumed to be 0.01. The gas temperature is 300K with a pressure of 0.1MPa and electron energy of 1.5eV. As the initial condition, we assume that the electron density and the atomic ion density are equal to each other and uniformly distributed in the discharge region $n_{\mathrm{e}}(r,0) = n_{\mathrm{i}}(r,0) = 10^7\mathrm{cm}^{-3}$, while the molecular ion density and the excited atom density are both $10^2\mathrm{cm}^{-3}$. The spacing between the two coaxial electrodes is 0.6cm; the outer radius of the inner electrode is $R_0 = 0.1$ cm, and the inner radius of the outer electrode is $R_2 = 0.7$ cm. The thickness of the quartz glass covering the outer electrode from inside is 0.1cm and its relative permittivity ε_{b} is 7.5, so the discharge gap is as wide as 0.5cm, and the axial length of the discharge installment is assumed to be $L = 10$ cm. A sinusoidal voltage is externally applied to the inner electrode, its amplitude and frequency are 2kV and 50kHz, respectively. After twenty discharge cycles, the system enters a relatively steady state.

Figure 2 shows the temporal evolution of the total discharge current and the gas voltage during a typical cycle. It can be seen that there is one current peak in each half cycle of the applied voltage. Different from the parallel-plate configuration, the current peak in various half periods loses its original shape. The current maximum of 0.48A in the first half is different from the second, which is only 0.14A. In addition, the pulse width of the discharge current in the latter half period is wider than that in the former. In the former half period, the outer cylindrical electrode is the discharge cathode. It is due to the fact that in the first half, the discharge cathode is the outer electrode with a big radius so that the volume of ionization region in the cathode sheath is also very large, leading to a strong current gathering; while in the latter half pe-

riod, the discharge cathode is the inner wire electrode with a very much smaller radius. Although in the latter case the sheath electric field is much stronger than that in the former, the volume of the ionization region is however so small that it leads to a smaller current peak. The solid line in Fig.2 represents the time-evolution of the gas voltage with the applied voltage during a typical cycle. At the initial moment, the applied voltage is zero, and the gas voltage is not zero but equal to the memory voltage produced by the charged particles accumulated on the dielectric. As the applied voltage rises, the gas voltage increases until reaching the breakdown voltage. Then the gas is punctured and discharge starts. Meanwhile, the charges accumulated on the dielectric produce a reverse electric field, making the gas voltage drop and leading to a termination of the gas discharge, as shown in Fig.2. Since the puncture time is very short, it restrains the free growth of the discharge current and avoids the emergence of arc discharge. In the latter half period, due to the reversal of the applied voltage, the electric field produced by the accumulated charges has the same direction as the applied field, so it reduces the threshold applied voltage for starting the next discharge. Furthermore, since the breakdown during the latter half period happens in the cathode sheath near the inner wire electrode, where the electric field is strong, correspondingly it is easier to puncture, and therefore the breakdown voltage in the latter half period is lower than that in the former half period. As a result of the higher discharge current during the former half period, the accumulation speed of charged particles on the dielectric barrier is fast too. Then the gas voltage drops rapidly and the discharge is suppressed quickly, and consequently the discharge current pulse is narrow. However, during the latter half period, since the discharge current is low, the accumulation speed of charged particles on the dielectric is also low. Thus the gas voltage changes slowly and its suppressing effect on discharge is small, so the current pulse is wide.

Figure 3 describes the evolutions of the surface density of charged particles accumulated on the dielectric and the discharge current as functions of time. The dielectric is affixed to the outer electrode. During the first half period of the applied sinusoidal voltage, the outer electrode is the cathode and the electric field points to it. Then the positive ions are accumulated on the dielectric barrier. When the gas discharge is ignited, the gas produces a large number of ions flowing to the cathode and accumulating on the dielectric, corresponding to the ascending part in Fig.3. However, during the latter half period, the inner electrode is turned to be a cathode and the electric field also points oppositely. Then electrons are accumulated on the dielectric barrier. When the gas punctures, it produces plenty of electrons flowing to the outer electrode. Since the discharge current is relatively small, the surface charge density accumulated on the barrier changes quite slowly.

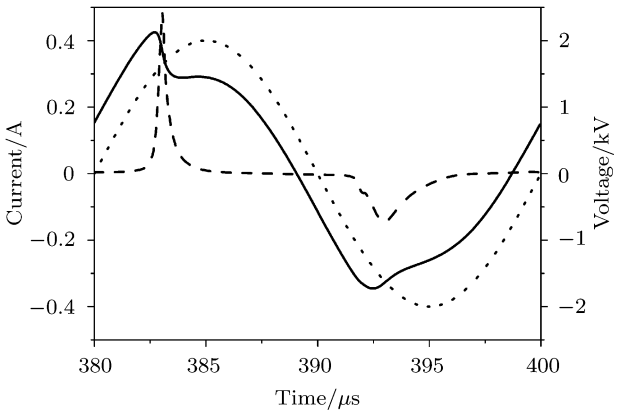


Fig.2. Evolution of the total discharge current and gas voltage in a typical cycle. The dashed curve represents the discharge current, the solid one represents the gas voltage and the dotted one represents the applied voltage.

Figures 4(a) and 4(b) illustrate the spatial distributions of the electric field, the ion, and the electron as well as the excited atom densities when the discharge current reaches its positive or negative maximum during the cycle. It can be seen in Fig.4(a), when the discharge happens in the former half period, the cathode sheath is formed near the dielectric barrier covering the outer electrode. There obviously exist a cathode fall, a negative glow region, a Faraday dark region, and a plasma positive column. This shows a similar feature to the typical glow discharge at low pressures. In the cathode fall, the electric field can be up to 23kV/cm and then decreases linearly from the cathode. The maximal ion density in this region is $4.7 \times 10^{11}\mathrm{cm}^{-3}$ and the width of the cathode fall is about 0.05cm. The width of the negative glow region and the Faraday dark region is about 0.15cm. The electron density shows a negative glow region with a peak value of $1.4\times10^{11}\mathrm{cm}^{-3}$. In other words, when the current reaches a peak during the former half period, the maximal electron density does not occur near the sheath but near the inner electrode. Due to the axial symmetry, the current density near the inner wire electrode is the highest. In the plasma positive col-

umn, the electric field is quite low, about 3kV/cm. The electron and ion densities are nearly equal to each other. Due to the asymmetry of discharges, the densities are not uniform in the plasma region but increase gradually from the outer to the inner electrode. Figure 4(b) indicates that during the latter half period when the current reaches the maximum, the cathode sheath is formed near the inner electrode. Obviously there exist the cathode fall, the negative glow region, and the positive column. In the cathode sheath, the electric field intensity is 27kV/cm in maximum and shows a tendency to reduce linearly. The thickness of the sheath is about 0.03cm and the ion density can be up to $4 \times 10^{11}\mathrm{cm}^{-3}$. The maximal electron density of $6 \times 10^{10}\mathrm{cm}^{-3}$ appears at the boundary near the sheath. In the plasma positive column, the electric field intensity is small and keeps almost steady; while the electron and ion densities are equal to each other, i.e. nearly 4×10^{10} cm^{-3}. The distribution of the excited atom density does not change too much during the former and the latter half periods. The maximal densities (about $8 \times 10^{11}\mathrm{cm}^{-3}$) both appear in the region near the inner wire electrode. The excited atom density decreases in the direction from the inner to the outer electrode.

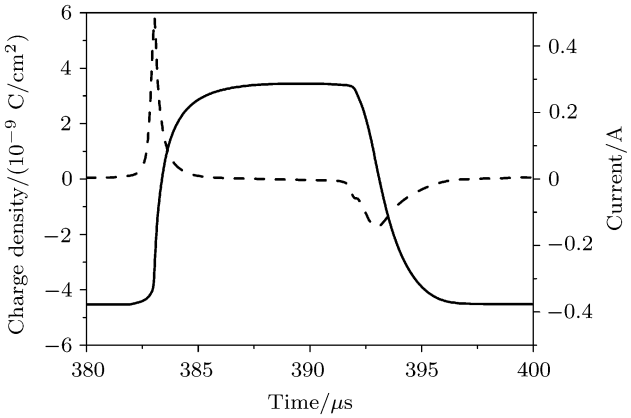


Fig.3. The surface density of charged particles and discharge current in a cycle. The solid curve represents the surface density of charged particles, and the dashed one represents the discharge current.

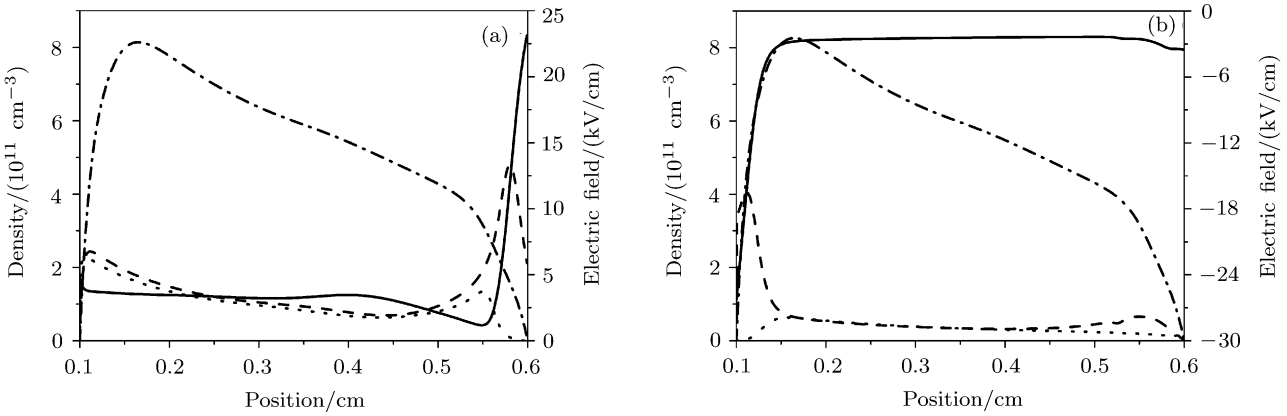


Fig.4. The spatial distribution of the electric field and densities of particles when the current reaches its maximum. The solid curve represents the electric field, the dashed one represents the ion density, the dotted one represents the electron density, and the dot-dashed one represents the excited atom density.

Figures 5(a) and 5(b) show the spatial distributions of the calculated source terms of direct ionization and other ionization on the right side of Eq.(1) when the current rises to its maximum. The other ionization includes the main penning effect and the excitation ionization. It can be seen that at the maximal current, the direct ionization plays the main role in the ionization source terms, three orders of magnitudes higher than the other ionization. Along with the alternation of the discharge cathode during the former and latter half periods, the peak value of the direct ionization appears in the corresponding cathode sheath, while the maximum of the other ionization, mainly the penning effect, does not, but it is mostly distributed in the region near the inner wire electrode all the time. Although the excited atom density has the same order as the electron and ion densities, as shown in Fig.4, it is not high enough to make the penning ionization comparable to the direct ionization. Therefore, the other ionization cannot play the main role in ionization. In calculations, the electron temperature is assumed to be constant, 1.5eV. However, the fact is that in the kinetic model the electron temperature can be as high as 10eV near the temporary cathode in the sheath re-

gion and as low as 1eV in the positive column, then the other ionization may be higher in the sheath and lower in the plasma column.

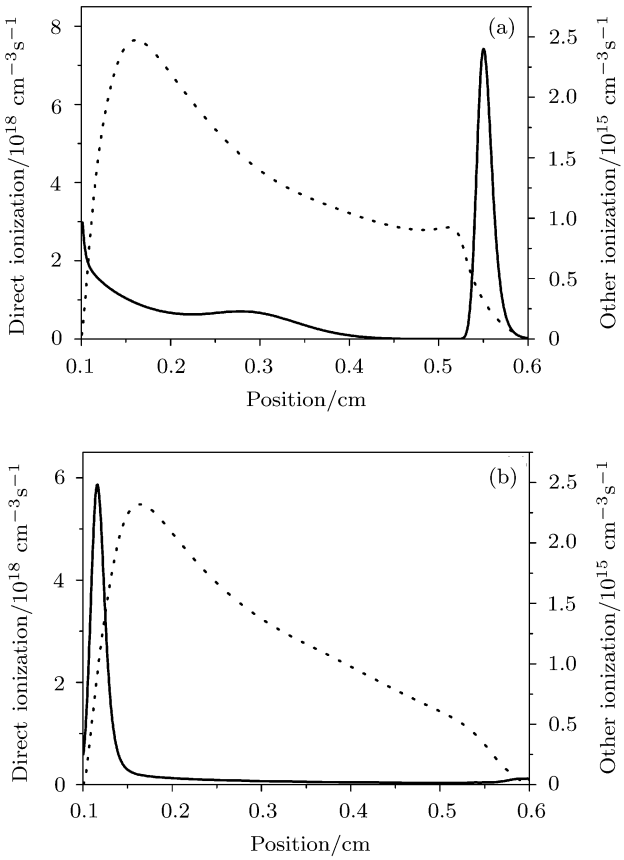


Fig.5. Calculated source terms of direct ionization and other ionization in pure helium. The solid curve represents direct ionization and the dotted one represents the other ionization.

Figure 6 shows the comparison of electrical characteristics between the following two discharge configurations: only the outer cylindrical electrode covered with the dielectric or only the inner wire electrode covered with dielectric. It can be seen that under the same discharge conditions, there is a great difference in the current amplitude and the gas breakdown point between the two discharge configurations. During the former half period of the applied voltage, the discharge happens early in the configuration of only the outer cylindrical electrode covered with dielectric, but late in the configuration of only the inner wire electrode covered with the dielectric. However, during the latter half period, the situation is opposite; the discharge happens early in the configuration of only the inner wire electrode covered with dielectric. In the dielectric barrier discharge, a great number of charged particles produced at the puncture time drift toward the two electrodes under the action of the applied electric field and accumulated on the surface of the dielectric. The higher the surface density of charged particles accumulated on the dielectric, the stronger the enhancement of the applied field during the next half period, and thus the earlier the gas break down.

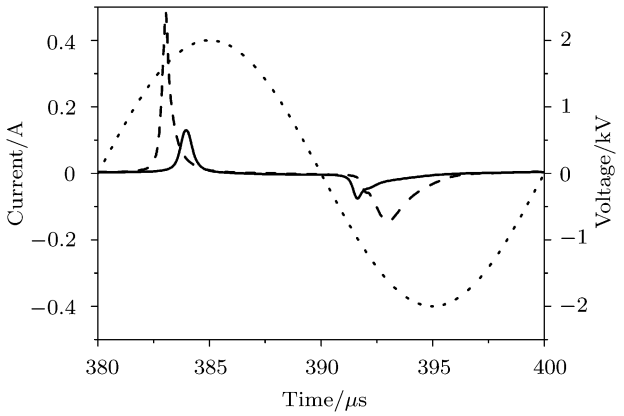


Fig.6. Electric characteristics in different barrier discharge configurations. The dashed curve represents only the outer electrode covered by the dielectric, the solid one represents only the inner electrode covered by the dielectric, and the dotted one represents the applied voltage.

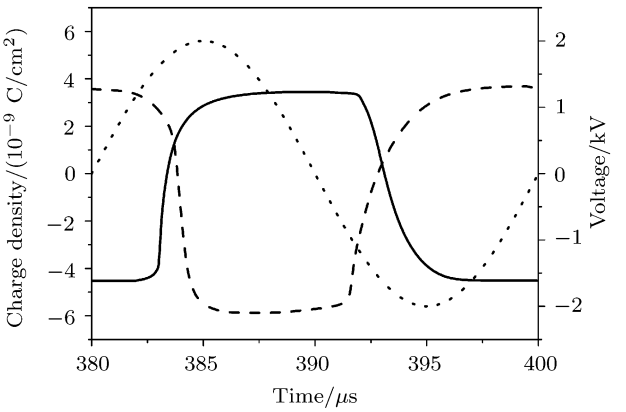


Fig.7. Surface density of charged particles accumulated on the dielectric in different discharge configurations. The solid line represents only the outer electrode covered by the dielectric, the dashed one represents only the inner electrode covered by the dielectric, and the dotted one represents the applied voltage.

In Fig.7 we can see that during the former half period of the sinusoidal voltage, for only the outer cylindrical electrode covered with the dielectric, the surface density of electrons accumulated on the dielectric is much higher, about 4.5×10^{-9}C/cm^2, so the discharge happens earlier, while in the other case, the surface density of positive charge is just about 3.5×10^{-9}C/cm^2, so the discharge happens later. However, during the latter half period, the gas breaks down early in this case because the surface density of electrons accumulated is far higher,

nearly 6.0×10^{-9}C/cm^2. It discharges late for the configuration of only the outer cylindrical electrode covered with the dielectric because of the low surface density of positive charge, about 3.5×10^{-9}C/cm^2. Due to the mobility of electrons, the surface density of electrons accumulated on the dielectric is always higher than that of the positive charge, as seen clearly in Fig.7, and therefore for the corresponding configuration with negative accumulated charge the current punctures earlier than the other case. Since the surface of the wire electrode is much smaller than that of the outer cylindrical electrode, the surface density of electrons accumulated on the dielectric for the configuration of only the inner wire electrode covered with dielectric is far higher, nearly 6.0×10^{-9}C/cm^2. Then, at the maximal current in the case of only the outer electrode covered with the dielectric, the sheath electric field is always stronger and the sheath thickness is always thinner than the other case, as shown in Fig.8. Thus the discharge current amplitude in Fig.6 is higher for this configuration, nearly to be as three times high as in the case of only the inner wire electrode covered with the dielectric. Moreover, the electric characteristics of the configurations of both the two electrodes covered with the dielectric are quite similar to that of the configuration of only the inner wire electrode covered with the dielectric.

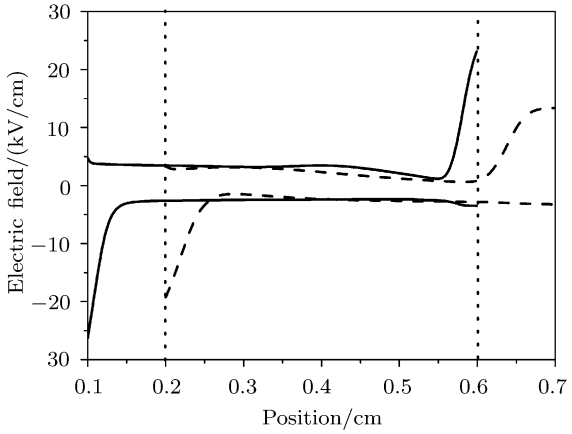


Fig.8. The electric field intensity in different configurations. The solid curve represents only the outer electrode covered by the dielectric, the dashed one represents only the inner electrode covered by the dielectric, and the dotted one represents the position of the dielectric barrier.

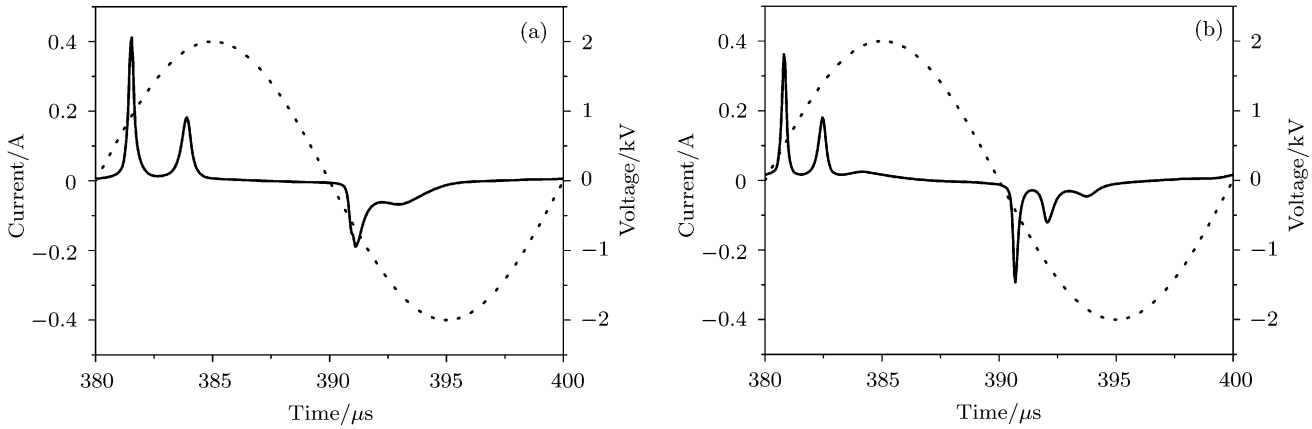


Fig.9. Electric characteristics in different discharge gap widths. (a) 0.3cm (b) 0.2cm. The solid curve represents the discharge current and the dotted one represents the applied voltage. Other parameters are the same as those in Fig.2.

With other discharge parameters being the same as discussed above but varying the gap width, the multiple current pulses occur as the discharge gap width reduces. With a gap width of 0.3cm, there exist two pulses during the first half period only. Reducing the gap width to 0.2cm, we find two pulses in both half periods. When the gap width narrows further, the distance the charged particles travel to the dielectric surface is also further reduced and the surface density of charged particles accumulated on the dielectric increases, leading to the growth of the memory voltage and the reduction of the threshold voltage to start the next breakdown. Thus the first breakdown happens earlier and earlier, as shown in Figs.9(a) and 9(b). As the applied voltage increases, the gas voltage reaches breakdown once more and the gas discharge happens once again during the latter half period.

4. Conclusions

Based on the one-dimensional and self-consistent fluid model, the characteristics of the dielectric barrier

glow discharge in pure helium at atmospheric pressure generated between two coaxial electrodes is investigated numerically. In calculation, we have considered the elementary ionization and excitation processes in pure helium. Under the drift-diffusion approximation, by solving the one-dimensional continuity equations for electrons, ions and excited atoms, together with the current conservation equation, the simulation results show the spatial–temporal distributions of the electric field and the electron, ion and excited atom densities, as well as the time evolutions of the discharge current, the gas voltage and the surface density of charged particles on the dielectric barrier. At maximal discharge current, there obviously exist the cathode fall, the negative glow region and the positive column, similar to the APGD with the dielectric barrier between parallel-plate electrodes. Though the axial symmetry of the wire-cylindrical electrodes system is found, the simulation results reveal that the peak discharge current, gas voltage and the electric field are asymmetric by comparing the first half cycle with the second. The influence of the way the dielectric covers the electrodes on discharge current characteristics is very significant. For the dielectric covering the outer electrode only, the discharge current amplitude is the highest, the gas punctures the earliest during the first half period and latest during the latter half, and the difference of the pulse widths is the most obvious. For the dielectric covering the inner electrode only, the discharge current is much smaller. Reducing the gap width causes the multiple current pulse discharge. As the gap width narrows, the number of current pulses increases.

References

[1] Kanazawa S, Kogoma M, Moriwaki T and Okazaki S J 1988 *J. Phys.* D **21** 836

[2] Yokoyama T, Kogoma M, Kanzawa S, Moriwaki T and Okazaki S J 1990 *J. Phys.* D **23** 374

[3] Yokoyama T, Kogoma M, Moriwaki T and Okazaki S J 1990 *J. Phys.* D **23** 1125

[4] Roth J R, Tsai P P, Liu C, Laroussi M and Spence P D 1995 *One Atmosphere Uniform Glow Discharge Plasma* (U.S. Patent 5) 414.304

[5] Tsai P P, Wadsworth L C and Roth J R 1997 *Textile Res. J.* **67** 359

[6] Montie T C, Kell-Wintenberg K and Roth J R. 2000 *IEEE Trans. Plasma Sci.* **28** 41

[7] Massines F, Rabehi A. Decomps P, Gadri R B, Segur P and Mayoux C 1998 *J. Appl. Phys.* **83** 2950

[8] Massines F and Gouda G 1998 *J. Phys.* D **31** 3411

[9] Kong M G and Deng X T 2003 *IEEE Trans. Plasma Sci.* **31** 7

[10] Wang Y H and Wang D Z 2003 *Acta Phys. Sin.* **52** 1694 (in Chinese)

[11] Wang Y H and Wang D Z 2005 *Acta Phys. Sin.* **54** 1295 (in Chinese)

[12] Wang X X, Lu M Z and Pu Y K 2002 *Acta Phys. Sin.* **51** 2778 (in Chinese)

[13] Wang X X, Li C R, Lu M Z and Pu Y K 2003 *Plasma Sources Science & Technology* **12** 358

[14] Fang Z, Qiu Y and Luo Y 2003 *J. Phys.* D **36** 29

[15] Wang Y H and Wang D Z 2004 *Chin. Phys. Lett.* **21** 2234

[16] Zhang Y T, Wang D Z, Wang Y H and Liu C S 2005 *Chin. Phys. Lett.* **22** 171

[17] Zhang G Q, Ge Y J, Zhang Y F and Chen G L 2004 *Chin. Phys. Lett.* **21** 2238

[18] SchÜtze A, Jeong J Y, Babayan S E, Park J, Selwyn G S and Hicks R F 1998 *IEEE Trans. Plasma Sci.* **26** 1685

[19] Ward A L, 1962 *J. Appl. Phys.* **33** 2789

[20] Shon J W and Kushner M J 1994 *J. Appl. Phys.* **75** 1883

[21] Stevefelt J, Pouvesle J M and Bouchoule A 1982 *J. Chem. Phys.***76** 4006

[22] Pouvesle J M, Bouchoule A and Stevefelt J 1982 *J. Chem. Phys.* **77** 817

[23] Deloche R, Monchicourt P, Cheret M and Lambert F 1976 *Phys. Rev.* A **13** 1140

[24] Yuan X and Raja L L 2003 *IEEE Trans. Plasma Sci.* **31** 495

[25] Shi J J and Kong M G J 2003 *Appl. Phys.* **94** 5505

[26] Zhu X M and Kong M G J 2005 *Appl. Phys.* **97** 083301

[27] Scharferter D L and Gummel H K 1969 *IEEE Trans. Electron. Devices* **ED -16** 64

[28] Kulikovsky A A 1994 *J. Phys.* D **27** 2856

[29] Xu X J 1996 *Discharge Physics of Gas* (Shanghai: Fudan University Press) 277 (in Chinese)

[30] Golubovskii Y B , Maiorov V A, Behnke J and Behnke J F 2002 *Proc. Hakone* 8 *th International Symposium on High Pressure Low Temperature Plasma Chemistry* **1** (Estonia) 48